Additive Manufacturing 66 (2023) 103452

Contents lists available at ScienceDirect

Additive Manufacturing

journal homepage: www.elsevier.com/locate/addma

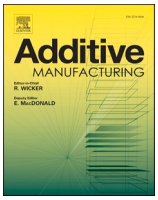

Stable large area drop-on-demand deposition of a conductive polymer ink for 3D-printed electronics, enabled by bio-renewable co-solvents

Geoffrey Rivers [a,*], Jonathan S. Austin [a], Yinfeng He [a,b], Adam Thompson [c], Negar Gilani [a], Nathan Roberts [c], Peng Zhao [a], Christopher J. Tuck [a], Richard J.M. Hague [a], Ricky D. Wildman [a], Lyudmila Turyanska [a,*]

[a] Centre for Additive Manufacturing, Faculty of Engineering, University of Nottingham, Nottingham NG8 1BB, UK
[b] Nottingham Ningbo China Beacons of Excellence Research and Innovation Institute, No. 211, Xingguang Road, Ningbo 315101, China
[c] Manufacturing Metrology Team, Faculty of Engineering, University of Nottingham, Nottingham NG8 1BB, UK

ARTICLE INFO

Keywords:
PEDOT:PSS
Conductive polymers
Inkjet printing
Large scale array
Heterostructures

ABSTRACT

Development of conductive polymer ink formulations with reliable jetting stability and physical properties could offer sustainable routes for scaling-up the 3D-printing of electronics. We report a new poly(3,4-ethylenedioxythiophene) polystyrene sulphonate (PEDOT:PSS) ink formulation, Ink_{CG}, using bio-renewable solvents dihydrolevoglucosenone (cyrene) and glycerol carbonate (GC) as an alternative to commonly used dimethyl sulfoxide (DMSO). These green organic co-solvents enhance jetting reliability and long-term stability of the ink and improve electrical properties of the deposited PEDOT:PSS layers, compared to the commonly used DMSO-containing ink formulations. We achieve large-area and high-fidelity electronic devices (array of 140 devices) with reproducible electrical performance through inkjet-based 3D printing. Enhanced performance stability is observed under cyclic bending, thermal annealing, UV or IR exposure, offering exciting opportunities for sustainable deposition of PEDOT:PSS for large-area 3D printing and its exploitation in heterostructures and flexible electronics.

1. Introduction

There is an increasing demand for ink formulations based on functional materials for inkjet-based 3D printing (IJ3DP) [1,2] that could offer opportunities for applications in electronics and optoelectronics [3,4]. IJ3DP enables low cost on-demand production of individually designed devices as well as large-area device arrays [5,6]. Of particular interest is inkjet deposition of poly(3,4-ethylenedioxythiophene) polystyrene sulphonate (PEDOT:PSS), which is a conductive polymer widely used in light emitting diodes (LEDs) [7], solar cells [8,9], photodetectors [10] and sensors [11,12]. PEDOT:PSS has been deposited mostly by spin-coating [13], screen-printing [14], meyer-bar coating [15,16] and electrohydrodynamic jet printing [17], and more recently by inkjet [18]. However, the processing reliability of inkjet printable PEDOT:PSS ink for device manufacture remains challenging [19] due to irregularity of the ink droplet placement, caused by small instabilities in jetting [20] and irregularity of printed PEDOT:PSS layer thickness, which can cause inconsistent conduction and inefficient operation of devices [21]. Despite the recently reported successful inkjet deposition of an array of PEDOT:PSS linear resistors over an area of approximately 9.5 cm × 4 cm [22], there remains a significant need for development of reliable formulations that are suitable for larger scale or many-layer inkjet printing required for manufacturing of electronics [23–25].

One of the key reasons for instability of PEDOT:PSS inks is the presence of DMSO, which is commonly used to improve PEDOT:PSS conductivity by screening the charges within PEDOT:PSS, thereby promoting entanglement and cohesion of neighbouring PEDOT:PSS colloidal particles [26,27]. Other additives, such as ethylene glycol (EG) derivatives, glycerol, dodecyl benzene sulphonic acid, dimethylformamide (DMF), water dispersed polyurethane (WPU), and others, were used for PEDOT:PSS formulations [13,15,28,29]. However, strong interactions between the additives and PEDOT:PSS may contribute to increased crusting at nozzles or formation of gel precipitates, both of which result in printing instability of DMSO-containing inks. The resulting limited jetting stability inhibits control of positional accuracy and jetting time, which are required to achieve scalable 3D printing of

* Corresponding authors.
E-mail addresses: Geoffrey.Rivers@nottingham.ac.uk (G. Rivers), Lyudmila.Turyanska@nottingham.ac.uk (L. Turyanska).

https://doi.org/10.1016/j.addma.2023.103452
Received 30 March 2022; Received in revised form 20 January 2023; Accepted 13 February 2023
Available online 14 February 2023

PEDOT:PSS for additive manufacturing of electronics (AME) [24,25]. In recent years, cyrene and GC have been proposed as renewable and biocompatible solvents to replace DMSO in biomedical applications [30,31] and could also offer new opportunities for PEDOT:PSS formulations.

In this work, we report a novel PEDOT:PSS ink formulation (Ink_{CG}) using the green renewable solvents cyrene and glycerol carbonate (GC) that exhibits improved jetting stability and suppressed coffee ring formation during drying, hence enabling deposition of more uniform layers. The deposited Ink_{CG} layers have enhanced electrical conductivity (about 200 S•cm^{-1}) compared to the DMSO-based formulation, and optimisation of the printing strategy reduced the surface texture parameter to Sa = 16 nm. Improvement in the conductivity of these layers is demonstrated under exposure to different environments, such as air, optical excitation with UV and IR light, thermal treatment, and deformation (1750 bending cycles). We explore the potential application of Ink_{CG} for deposition of large-area arrays of intricate electrode designs onto flexible substrates (140 devices in a 10 cm × 6.3 cm area), enabling a route of large-area inkjet PEDOT:PSS device production. Enhanced printing performance, storage stability and device performance offer exciting opportunities for the use of PEDOT:PSS in heterostructures, as demonstrated here through co-printing with Ag-nanoparticle and graphene inks, for applications in functional devices and flexible electronics produced by IJ3DP. Fig. 1

2. Materials and methods

2.1. Materials

Conductive polymer inks were formulated using a commercial aqueous suspension of PEDOT:PSS (1.1 wt%, Clevios PH 1000) diluted by combinations of DMSO, diethylene glycol (DEG), tetraethylene glycol dimethyl ether (Tetraglyme), 3-glycidyloxypropyl trimethoxysilane (GOPS), cyrene, GC, Triton X-100 (Tx), polysorbate 80 (Tween-80), and ultrapure deionised water (DI). Clevios was purchased from Ossila, while all other chemicals were purchased from Sigma Aldrich; all were used as received.

2.2. Ink formulation

To produce ink formulations, additives were mixed under stirring at 400 RPM for 15 minutes before adding PEDOT:PSS (Table 1 and Supplementary Information SI1, SI2). Following another 20 hours stirring at room temperature, inks were filtered with a syringe filter (0.45 µm, Millipore Millex-LCR hydrophilic), loaded into a Dimatix inkjet print cartridge (DMC-11610, Fujifilm, 21 µm nozzle diameter). The printhead nozzles were primed and purged with ink while inverted to expel large air pockets from the ink tank before installing the cartridge in the printer.

2.3. Jetting performance analysis with liquid handler

An automated liquid handler (Hamilton Microlab STAR) with customised software and a high-sensitivity mass scale was used for measurements of viscosity,η, and the surface tension, γ [32]. These were used to calculate the Z parameter (Table 1): printable inks should satisfy the following relationships: $R_e = \rho V d/\eta > (2\ O_h^{-1})$; $R_e^{5/4} < (50\ O_h^{-1})$, and $1 < Z < 10$, where R_e is Reynolds number, $O_h$is Ohnesorge number ($O_h = \eta/\sqrt{\gamma\rho d}$), $Z = O_h^{-1}$; ρ is density, and V is droplet velocity.

2.4. Inkjet printing

A piezo-based inkjet printer (DMP 2830, Fujifilm) was used to

Table 1
Composition, viscosity, surface tension, and printability Z parameter of the investigated inks.

		Ink_{DMSO}	$Ink_{DMSO+DEG}$	Ink_{CG}
Composition (wt%)	PEDOT:PSS dispersion	46.2	44	38.4
	Water	46.7	44	55.2
	DMSO	5.1	5	-
	Tetraglyme	0.5	0.5	-
	Tx	0.5	0.5	-
	GOPS	1	1	0.45
	DEG	-	5	-
	Cyrene	-	-	4.3
	GC	-	-	0.85
	Tween-80	-	-	0.8
Viscosity, η (cP)		10.1	10.1	8.6
Surface tension, γ (mN•s^{-1})		35.6	36.1	41.5
Z parameter		2.7	2.7	3.4

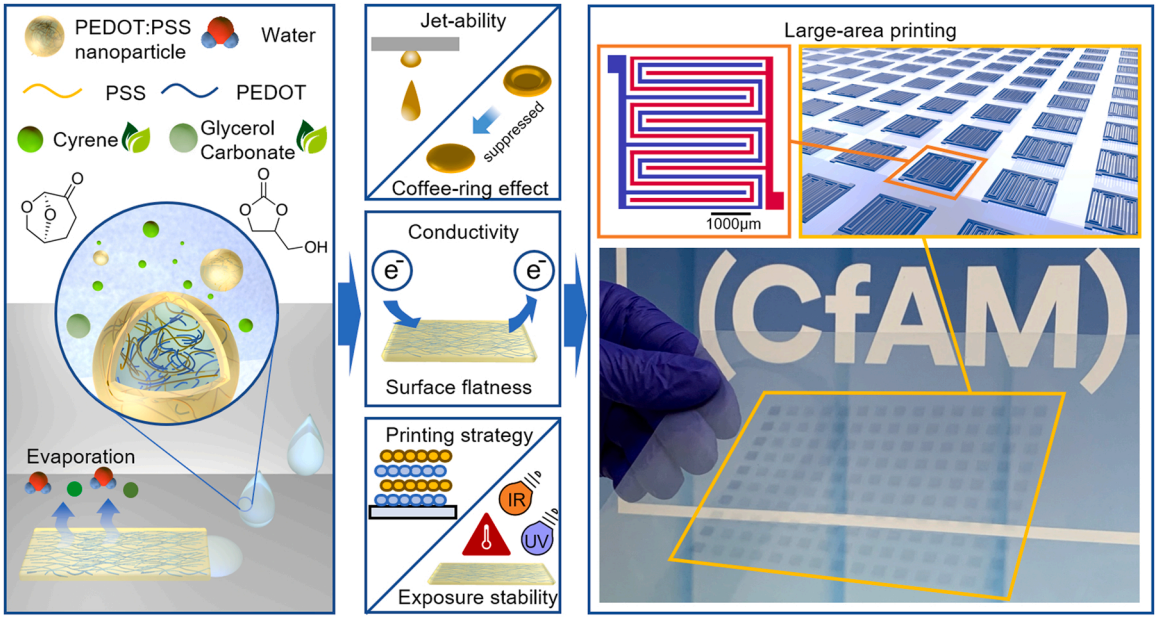

Fig. 1. Schematic illustration of the formulation of PEDOT:PSS ink utilising cyrene and GC for improved jetting and printing performance, conductivity, morphology and stability of the printed layers. Design and a photograph of the large-scale printed array of electrical PEDOT:PSS devices.

deposit inks onto borosilicate microscope slides (Fisher Scientific) or polyethylene naphthalate (PEN) flexible film. The substrates were cleaned by sequential washings of detergent water, DI-water, ultrapure water, acetone, and isopropanol. In this system, the x-axis is defined as the direction of printhead travel along which a swath is printed, while the y-axis is defined as the direction of the substrate movement along which sequential swaths are arrayed. The following printing parameters were used in this work: single nozzle, droplet spacing of 34 μm, substrate temperature of 45°C, and number of layers $n_L = 1, 2, 4, 6$. For the aligned print strategy, the swaths of each layer were aligned and printed directly on top of one another. For the cross-ply strategy, the specimens are rotated 90° after each layer (alternating clockwise and counter-clockwise rotation). For the offset strategy the print position was offset one half the drop spacing in the y-axis between layers. A large-scale array of serpentine electrodes for use in capacitive sensing, adapted from Rivadeneyra et al. [33], was printed onto PEN film substrates in two layers using the aligned print strategy.

2.5. Post-printing environmental treatments

Post-deposition thermal annealing was performed in a natural convection oven (Carbolite Gero PN) at $T_{ann} = 150°C$ for 30 minutes, with longer durations used to assess the stability. Effect of exposure to infrared annealing (IR, 600 W, 1.3 μm twin tube lamp Heraeus Noblelight Ltd., $P = 60$ mW•mm^{-2} at specimen) and ultraviolet light (UV, FireFly 25x10AC395-4W lamp, $\lambda = 395$ nm, $P = 3.7$ mW•mm^{-2}) was also assessed.

2.6. Surface texture characterisation

A Nikon Optical Microscope with 5 × and 20 × magnification was used for optical examination, with line width measurements made through image analysis in NIS Elements D software and calculated as mean ± 95% confidence interval for 30 measurements (6 printed lines, 5 measurements each). Surface topography was measured using coherence scanning interferometer (CSI, Zygo NewView NX2) [34] equipped with a white light source with a nominal $\lambda = 570$ nm, and 1 × and 1.4 × objectives (numerical aperture, NA, 0.04; lateral resolution, LR (Sparrow optical limit) 7.13 μm; PS 1.56 μm; field of view, FoV 6.15 mm × 6.15 mm), 5.5 × objective (NA 0.15, LR 1.90 μm, PS 1.56 μm, FoV 1.56 mm × 1.56 mm), and 20 × objective (NA 0.40, LR 0.71 μm, PS 0.43 μm, FoV 0.43 mm × 0.43 mm). Surface texture data were analysed using software TopoScan and MountainsLab (DigitalSurf). The following parameters were assessed: the arithmetical mean deviation of the assessed profile, *Ra*; root mean square deviation of the assessed profile, *Rq* and the areal analogues of these *Sa* and *Sq*, were calculated in MountainsMap [35]. All *Ra* parameters were generated using the following filtering conditions, in accordance with ISO 3274: evaluation length 0.4 mm, sampling length 80 μm, $\lambda s = 2.5$ μm, $\lambda c = 80$ μm. We estimate arithmetical mean height of the scale limited surface, *Sa* surface texture parameter [36] with S-filter nesting index = 2.5 μm, L-filter nesting index = 1 mm.

2.7. Electrical characterisation

PEDOT:PSS was printed with square geometry (1.24 mm × 1.24 mm) for 1, 2, 4 and 6 layers. For van der Pauw (vdP) measurement, contacts were produced using conductive Ag paint (RS PRO, 186-3600). For all vdP measurements, the contact size was significantly smaller than the gap between the contacts (see Supplementary Information SI3, Fig. S2). A source metre Keithley 2400 was used for measurements.

2.8. Cross-sectional SEM, TEM and EDX

Printed heterojunction specimens (Ink_{CG} PEDOT:PSS on inkjet printed graphene) were characterised by cross-section SEM and EDX elemental mapping. Inkjet graphene was 10 layers, and was formulated, printed, and post-treated as previously published before printing 10 layers of Ink_{CG} [37]. Zeiss crossbeam 550 (Oberkochen, Germany) was used to cross-section the samples and images were acquired using the Secondary Electrons Secondary Ion (SESI) detector operated at 5 kV and 300 pA with a working distance of 5 mm. The elemental composition of the surface was identified via an Energy-Dispersive X-ray (EDX) spectrometer (Oxford Instruments) at a working distance of 5 mm and beam voltage of 10 kV. TEM images, STEM images, and TEM-EDX were acquired on a JEOL 2100Plus equipped with a Gatan Ultrascan1000XP CCD camera, JEOL STEM detectors, and an Oxford Instruments XMax100TLE spectrometer.

2.9. Statistical analysis

For *Ra* data, a total of 30 measurements were made for each presented data point, obtained from 3 printed lines with 10 measurements each across their length, and error bars represent the 95% confidence interval of the pooled data. For surface slope estimates, error estimates are standard error for least-square fits of the central region of a representative printed line. For line width measurements, a total of 30 measurements were made for each presented data point, obtained from 6 printed lines with 5 measurements each across their length; error bars represent the 95% confidence interval of the pooled data. For conductivity measurements, error bars represent the 95% confidence interval of 4 specimen replicates. For electrical stability measurements, error bars represent 95% confidence interval for 3 specimen replicates. For bending stability, error bars were calculated from linear fitting of $I(V)$s and by the range of the resistance recorded in-situ (with applied $V_{sd} = 100$ mV) during the last 5 bending cycles before the $I(V)$ was measured.

3. Results and discussion

3.1. Formulation of inks

DMSO-based PEDOT:PSS inks (Ink_{DMSO}) were used as the control formulation, while $Ink_{DMSO+DEG}$ contained an additional 5 wt% DEG to investigate improvement of printing stability and conductivity. Ink_{DMSO} and $Ink_{DMSO+DEG}$ contain DMSO, known to be a conductivity-improving additive for PEDOT:PSS that promotes agglomeration and gelation of the PEDOT:PSS during drying [26], as well as Tetraglyme, Tx, and GOPS (Table 1), respectively intended as a flexibility enhancer [38], surfactant [39], and cross-linker [40]. In our preliminary studies we investigated the effect of co-solvents and additives on jetting stability (Supplementary Information SI1). DEG was used to improve jetting stability by reducing evaporation, and to improve conductivity by promoting an aligned microstructure in the dried ink [41]. In Ink_{CG} the Tx surfactant is replaced with biocompatible surfactant Tween80, the concentration of GOPS is reduced, and no Tetraglyme was used. Ink_{CG} also contains cyrene and GC instead of DMSO, which are renewable and have not yet been reported as a PEDOT:PSS additive. We note, that Ink_{DMSO} was investigated with and without GOPS, and no significant difference in stability during storage and ink-jetting was observed. In this work we use Ink_{DMSO}, which has similar composition to commercially available inks, to benchmark our results.

We found that Ink_{CG} achieved stability of over 4 days if stored at room temperature under stirring, or unstirred at $T = 4°C$ for up to 5 days and re-stirred for 2 hours before use. This is a significant improvement *c. f.* Ink_{DMSO} and $Ink_{DMSO+DEG}$, where the inks were not printable after overnight storage in either condition.

3.2. Morphology of inkjet printed PEDOT:PSS

Deposition with a single nozzle, droplet spacing of 34 μm and substrate temperature of 45°C was used for all samples reported here. Profiles extracted from areal CSI measurements (across the length and

width of the lines, Fig. 2a,b) revealed visible differences between the morphology of the layers on PEN substrate produced using three studied inks. Ink_{DMSO} and $Ink_{DMSO+DEG}$ show a pronounced increase of thickness at the edge of the printed line even for 6-layer samples, caused by non-uniform deposition of PEDOT:PSS due to coffee ring effect [42].

The profiles measured for Ink_{CG} revealed that the new green solvent formulation has suppressed the coffee ring effect (Fig. 2a). Ink_{DMSO} also displays an increasing thickness (slope 118 ± 0.7 nm•mm^{-1}, $N = 1990$) along the print direction in the central segment, excluding the coffee ring region, whereas $Ink_{DMSO+DEG}$ and Ink_{CG} display significantly flatter central slope (44 ± 2.7 nm•mm^{-1} for $N = 1850$, and 5 ± 0.7 nm•mm^{-1} for $N = 1500$, respectively). For Ink_{CG} a marked suppression of coffee ring effect is observed for $n_L \leq 6$ (Fig. 2b), likely due to the higher viscosity of cyrene (14.5 cP) and GC (85.4 cP) compared to DMSO (2.0 cP) [43]. The thickness of the Ink_{CG} line decreases at the end of the printed line (about 20% of the overall length), which we suggest is caused by the redistribution of the ink due to surface tension. This is where the already deposited and drying ink pulls the subsequently deposited ink drops towards the start of the swath, minimised by the viscosity of the green solvents and with the effect apparent at the end of the printed line [44].

The ISO 4287 *Ra* parameter [45] (Fig. 2c) extracted from the central part of the sample (80% of the length and width, to avoid contributions from the coffee ring effect) revealed that Ink_{DMSO} and Ink_{CG} have comparable *Ra* values (respectively $Ra = 6 \pm 0.4$ nm and $Ra = 5 \pm 0.4$ nm for $n_L = 1$; respectively $Ra = 5 \pm 0.4$ nm and $Ra = 7 \pm 0.6$ nm for $n_L = 6$). In contrast, the *Ra* value for $Ink_{DMSO+DEG}$ increases from $Ra = 8 \pm 0.4$ nm for $n_L = 1$, to $Ra = 24 \pm 1.1$ nm for $n_L = 6$, likely due to phase separation of the PEDOT:PSS induced by the DEG during drying [46]. Hence only Ink_{DMSO} and Ink_{CG} were selected for further studies.

Optical microscopy images of printed lines on PEN and glass substrates reveal differences in the width of single lines between the two inks. On PEN, Ink_{DMSO} has the width $w = 63 \pm 2$ µm for single droplet wide, single layer horizontal lines (Fig. 2d). With additional printed layers, the width increases sharply to $w = 75 \pm 3$ µm for $n_L = 2$ and remains unchanged up to $n_L = 6$, where $w = 74 \pm 2$ µm. The width of the single line printed on PEN using Ink_{CG} revealed $w = 40 \pm 2$ µm for one printed layer, which is comparable to the minimal size expected for the used drop volume (10 pL). The line width increased linearly with increasing number of layers to reach the value of $w = 84 \pm 6$ µm for $n_L = 6$, comparable to Ink_{DMSO}. On glass, Ink_{DMSO} presented broad lines with $w = 70 \pm 5$ µm for all $n_L \leq 6$, while Ink_{CG} formed narrower lines with $w = 44 \pm 2$ µm for $n_L = 1$ increasing to $w = 58 \pm 3$ µm for $n_L = 6$. The ability to reliably deposit narrow lines with PEDOT:PSS inks is critical to their use in printing of micro-scale electronic devices.

3.3. Optimisation of printing strategy to control layer morphology

Surface texture can be modified and controlled by the printing strategy. In the approach where each next layer's swaths are printed directly on top of and aligned with the previous layer's swaths (aligned layers), a wavy structure is produced (Fig. 3a). Hence, this and another two printing strategies were employed (Fig. 3a-c): aligned layers, cross-ply layers (90° rotation for each subsequent layer), and offset layers (each next layer was offset one half the drop spacing along the y-axis). CSI measurements (insets in Fig. 3a-c) revealed the printing strategy significantly affected surface texture with the wave-like pattern observed for standard print and plaid-like pattern for crosswise print, and reduced wave patterns for the offset strategy (see also Supplementary Information SI4, Fig. S3). For the aligned print strategy, the CSI measurements indicate surface pitting between printed swaths (Fig. 3a).

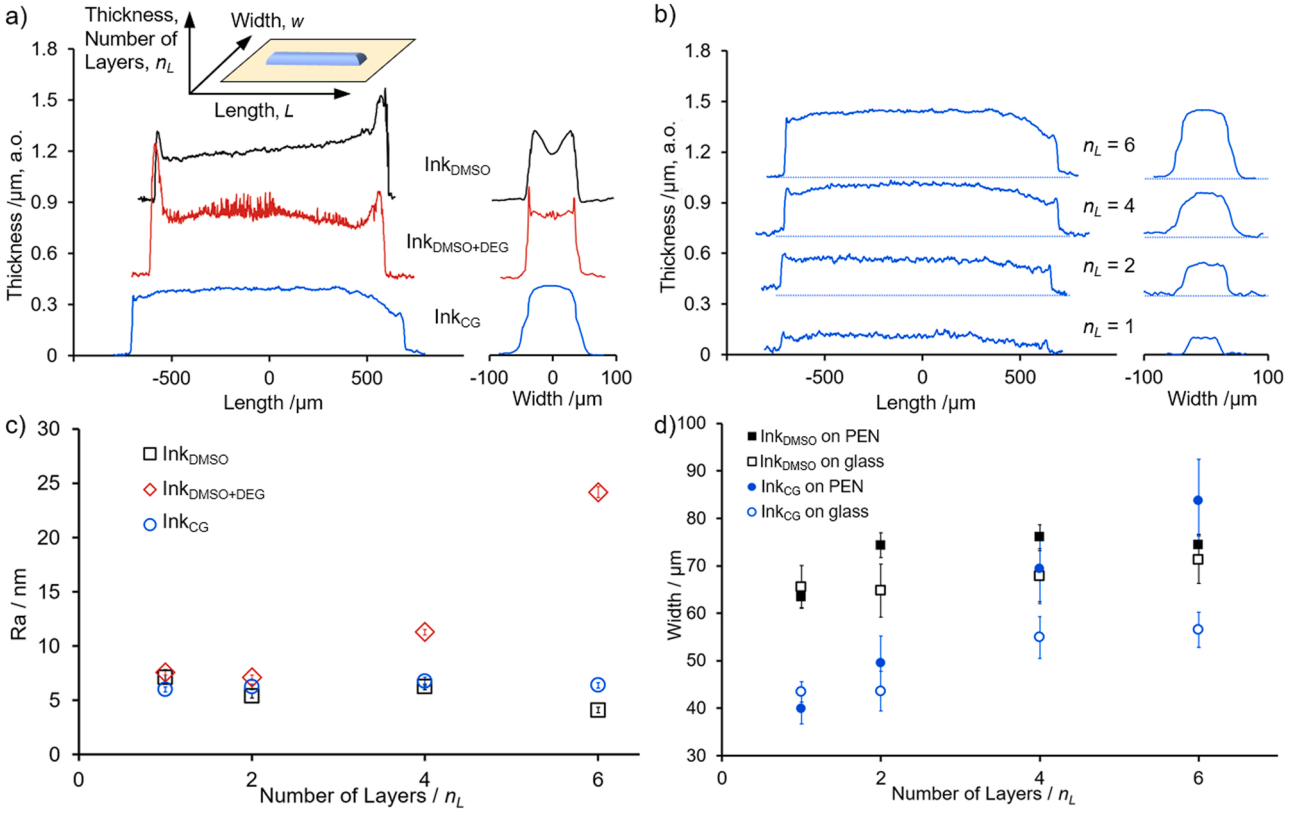

Fig. 2. a) Thickness profile along and across the length of printed lines, one droplet wide, for Ink_{DMSO}, $Ink_{DMSO+DEG}$ and Ink_{CG}, each printed $n_L = 6$ layers. Inset displays direction definitions of measurements; b) Thickness profile along and across the length of printed Ink_{CG} lines, one droplet wide, for $n_L = 1$, 2, 4, and 6; c) Dependence of *Ra* parameter on the number of printed layers for all three inks; and d) width, w, of lines printed from Ink_{DMSO} and Ink_{CG} on PEN and glass substrates for various numbers of layers. For the Ra values, error bars representing the 95% confidence interval, n = 30 measurements (3 printed lines, 10 measurements each). For line width measurements, error bars representing the 95% confidence interval, n = 30 measurements (6 printed lines, 5 measurements each).

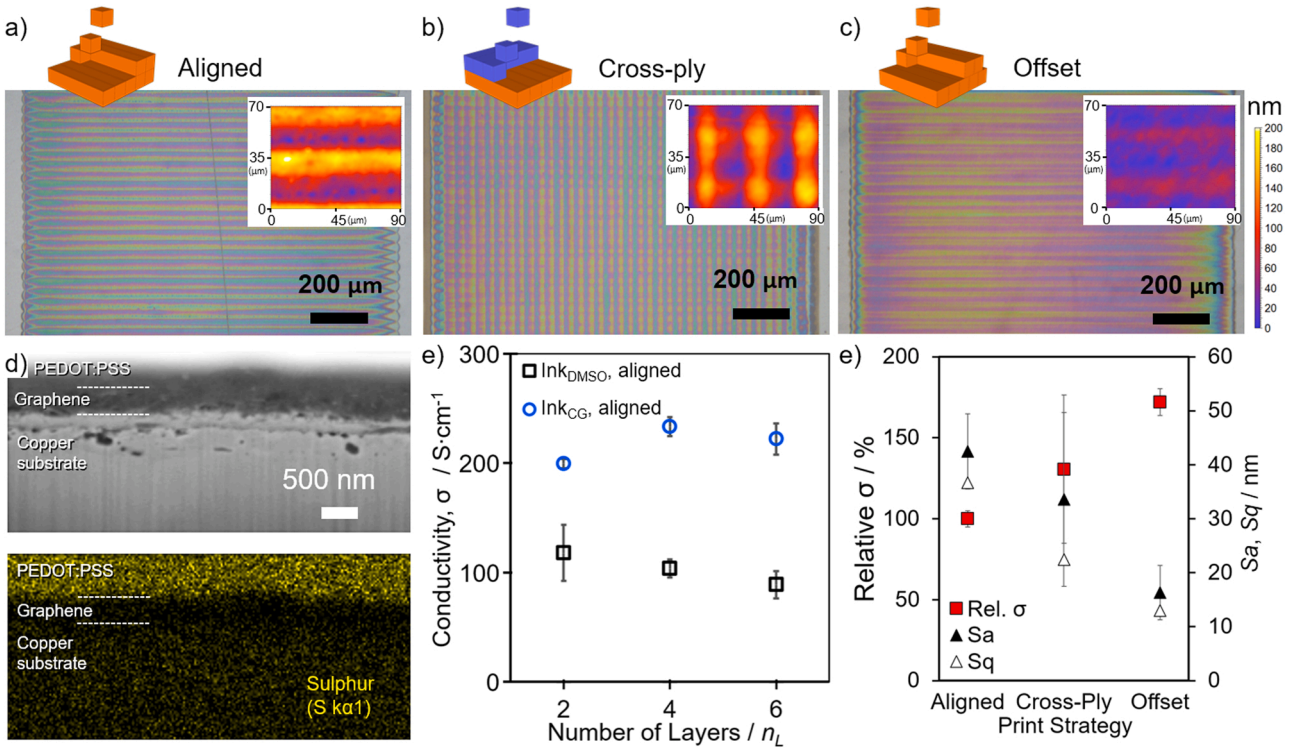

Fig. 3. Schematic representation of print strategy and optical micrograph of resulting Ink$_{CG}$ films for **a)** aligned printing, **b)** cross-ply printing, and **c)** offset printing. Insets of each display surface topology from CSI at higher magnification, 70 µm × 90 µm; **d)** A representative SEM image of Ink$_{CG}$ layer deposited on graphene and corresponding EDX elemental map (sulphur) showing continuous uniform PEDOT:PSS film ($n_L = 10$). **e)** Comparison of conductivity vs printed layers for Ink$_{DMSO}$ and Ink$_{CG}$ printed by aligned print strategies; **f)** Comparison of relative conductivity and waviness factors *Sa* and *Sq*, for Ink$_{CG}$ films, $n_L = 4$, printed with the three printing strategies. Relative conductivity has been normalised to conductivity of aligned print strategy. All error bars within are 0.95 confidence interval for 4 specimen repeats.

These are not formed in the cross-ply or offset strategies (Fig. 3b-c insets, and Supplementary Information S2, Fig. S2). Cross-sectional SEM and EDX studies of a line printed with Ink$_{CG}$ (Fig. 3d, Fig. S7-S8), confirm the formation of continuous uniform layer, with no internal voids and/or porosity, hence fulfilling the requirement for its application in vertical heterostructure devices for 3D-printed optoelectronics. We also note, that highly porous structures can be achieved by changing the formulation, as we demonstrate for Ink$_{Comm}$ structure, where regularly spaced 15 µm micro-pores were formed at 35 µm intervals (see Supplementary Information SI5, and Fig. S4).

The conductivity of Ink$_{CG}$ is greater by a factor of 2 (218 S•cm^{-1}) compared to Ink$_{DMSO}$ (103 S•cm^{-1}) (Fig. 3e, printed on PEN using the aligned strategy for n_L = 2, 4 and 6), demonstrating a significant improvement in PEDOT:PSS performance using cyrene and GC. For all studied inks the conductivity is independent of the number of printed layers. However, the conductivity of the Ink$_{CG}$ was affected by the printing strategy employed (Fig. 3e). A significant decrease in waviness was observed for offset-printed sample with $Sa = 16 \pm 5$ nm compared to $Sa = 43 \pm 7$ nm measured for standard print. The decrease in *Sa* is accompanied by an increase of the conductivity by a factor of 1.7, likely due to improved connectivity within the printed PEDOT:PSS film (Fig. 3 f). The achieved improvement of the morphology is of particular interest for applications of PEDOT:PSS in heterostructures, where control of layer thickness, low surface roughness and absence of pinholes or internal voids are required for optimal device performance [47]. We note, that the PEDOT:PSS Ink$_{Comm}$ where printed lines revealed the formation of microporous structures for $n_L = 2$, the voids and pores were filled by the next added layers leading to an increase of electrical conductivity.

3.4. Electrical stability during post treatment

During printing of heterostructures and operation of devices, printed PEDOT:PSS layers may be exposed to different environments such as long-term exposure to ambient conditions, exposure to UV when co-printed with photocured polymers (e.g. TPGDA [48]), and exposure to IR or thermal annealing when co-printed with nanoparticle based inks (e.g. AgNPs [49] and AuNPs [50]). Therefore, the stability of Ink$_{CG}$ with respect to the electrical properties at different environmental conditions (Fig. 4) were examined. The sheet resistance, *Rs*, was measured in van der Pauw configuration. Both Ink$_{DMSO}$ and Ink$_{CG}$ displayed a small change in sheet resistance after 2.5 hours of annealing at T_{ann} =140°C (Fig. 4a), with Ink$_{DMSO}$ demonstrating an increase from $Rs = 299$ Ω•sq^{-1} to 329 Ω•sq^{-1} and Ink$_{CG}$ from $Rs = 162$ Ω•sq^{-1} to 214 Ω•sq^{-1}. Further increase in annealing time up to 24 hours had no significant effect on *Rs*. In contrast, during the first 2 hours of IR exposure (Fig. 4b, solid lines) Ink$_{CG}$ displayed no significant change, while an increase of *Rs* was observed for Ink$_{DMSO}$, similar to changes seen during thermal annealing. For all tested IR exposure durations, the sheet resistance of Ink$_{CG}$ remained lower than that of Ink$_{DMSO}$. The stability observed indicated that the Ink$_{CG}$ is more suitable for multi-material designs requiring deposition of nanoparticle ink, where post-processing conditions would only have a small or negligible impact on its sheet resistance.

Both ink formulations demonstrated comparable stability under UV exposure (Fig. 4b and Supplementary Information SI6, Fig. S5), where about 2× increase of sheet resistance of Ink$_{CG}$ to 250 Ω•sq^{-1} was observed after 40 minutes exposure (~890 J•cm^{-2}). This UV exposure is comparable to that required for inkjet printing of over 1500 photocurable polymer layers using a Dimatix printer [51], and thus likely sufficient for inkjet deposition of 3D printed heterostructures and for deposition of electronic packaging layers. Long-term exposure to

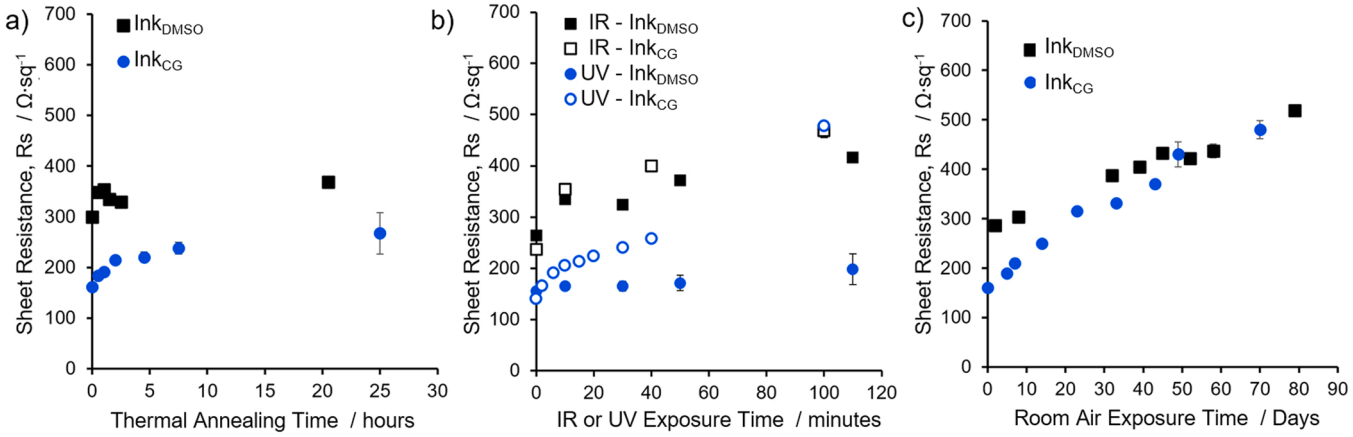

Fig. 4. Comparison of sheet resistance for Ink$_{DMSO}$ and Ink$_{CG}$ during exposure to a) thermal annealing (T_{ann} = 140°C), b) irradiation by IR and UV, and c) room air exposure over time, respectively. Error bars are 0.95 confidence interval and 3 repeats.

ambient conditions also affects the stability of electrical properties of both formulations (Fig. 4c) with *Rs* increasing by a factor of 2 after 24 days storage. This instability is likely due to the presence of oxygen and can be improved by sealing the PEDOT:PSS with surface capping to prevent oxidation (see Supplemental Information SI6, Fig. S5) [52].

3.5. Suitability for 3D printed heterostructures

To illustrate that improved stability of our Ink$_{CG}$ PEDOT:PSS films offers potential benefits in printed electronics applications, we produced proof of concept PEDOT:PSS heterostructures with commercial AgNP and graphene inks (Fig. 5a-b). In all structures, the sheet resistance of PEDOT:PSS after the deposition of a subsequent layer was comparable to that measured before, demonstrating the excellent potential for Ink$_{CG}$. A co-printed heterostructure of Ink$_{CG}$ and AgNP ink was successfully used to form a Hall bar geometry (Fig. 5b). Our preliminary work also indicates that non-commercial inks (e.g. perovskite nanocrystal inks, polyTPD inks) are also compatible with the Ink$_{CG}$ formulation. These studies performed for Ink$_{DMSO}$ (Supplementary Information SI7, Fig. S7) revealed some intermixing between the printed layers, which merits further investigations. To explore the potential for flexible electronics, a line of Ink$_{CG}$ (3 mm × 55 mm, n_L = 4) was printed on PEN substrate and

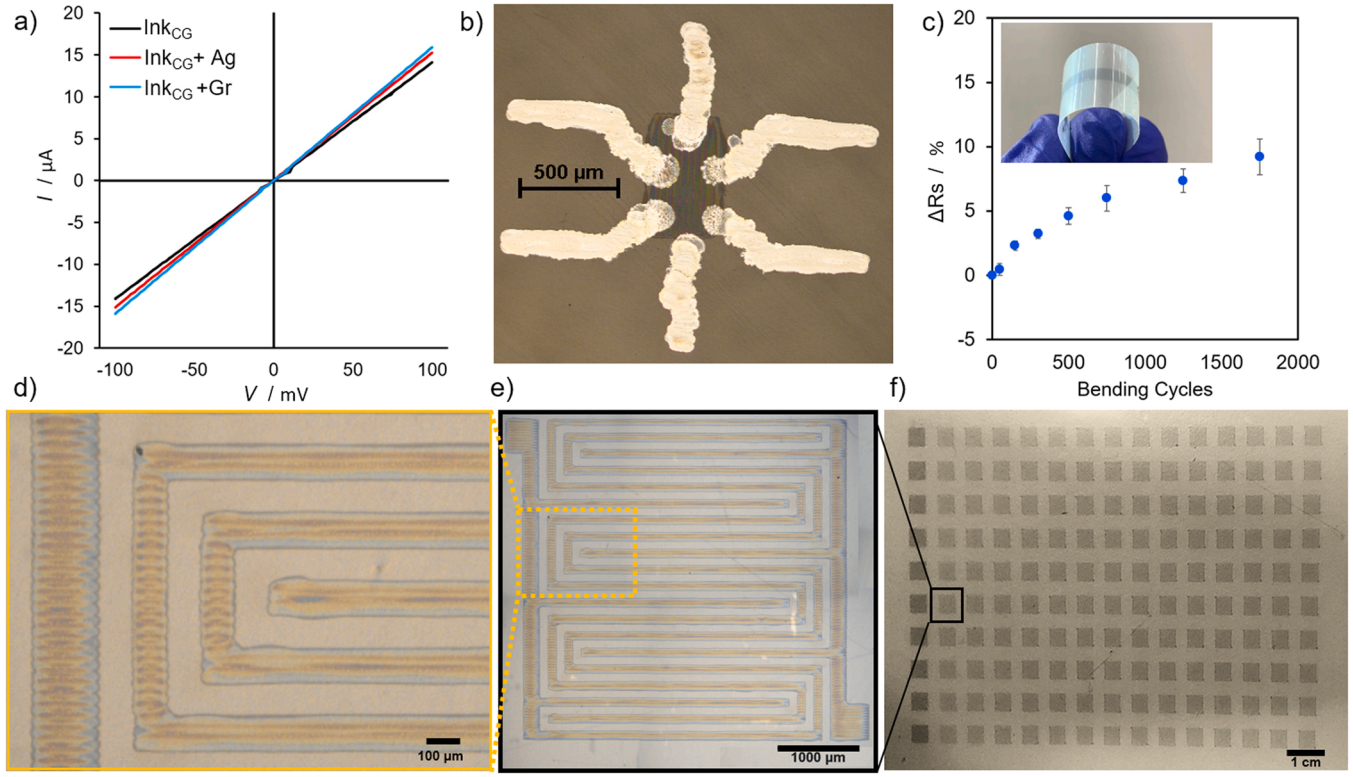

Fig. 5. a) Current-voltage *I*(*V*) characteristics for conductive lines of Ink$_{CG}$ on PEN, as printed, or over-printed with commercial inks as a heterostructure (AgNP ink or graphene ink); **b)** Example of a functional heterostructure: Ink$_{CG}$ rectangle n_L = 4, over-printed with AgNP traces in a Hall bar configuration; and **c)** Relative resistance of Ink$_{CG}$ line, n_L = 4, printed on PEN flexible substrate undergoing bending (bend radius = 1.4 cm). Inset: photograph of specimen in bending (see Fig. S6 for optical microscopy of Ink$_{CG}$ before and after bending); **d)-f)** close-up, single electrode unit and full array of 14 × 10 serpentine electrodes (contrast adjusted for visibility) printed using Ink$_{CG}$ with n_L = 2 on PEN substrate. Error bars were calculated from linear fitting of *I*(*V*)s and by the range of the resistance recorded in-situ (with constant V_{sd} = 100 mV) during the last 5 bending cycles before the *I*(*V*) measurement was taken.

subjected to bend testing (Fig. 5c), where only a 10% increase in sheet resistance was observed after 1750 cycles, indicating that Ink_{CG} may be applicable to future flexible electronics applications. Optical microscopy images of printed structures before and after cyclic bending (Fig. S6) revealed no visible morphological change in the PEDOT:PSS, hence confirming the improved stability of continuous layers fabricated using Ink_{CG} formulation.

3.6. Large-area printing of device arrays

The jetting stability achieved for the Ink_{CG} offers benefits for large-scale inkjet deposition (Fig. 5d-f). We printed an array of 14 × 10 serpentine electrodes with an area of 10 cm × 6.3 cm, of which microscopic inspection determined that 138 printed electrodes did not contain printing defects in the form of bulged lines, missing swaths, missing droplets, or misplaced droplets. Two electrodes contained printing defects in the form of bulging lines, though these did not result in short circuits and thus would retain their capacitive function. In comparison to the common printing defects observed during similar attempts of printing a single package of strain sensors (only 1.5 cm × 1.1 cm) using Ink_{DMSO} (Supplementary Information SI8, Fig. S9), this demonstrates that Ink_{CG} enables large-area printing of electronic traces over large areas.

3.7. Discussion

The PEDOT:PSS formulation developed in this work offers a new ink with improved jetting stability compared to typical formulations containing up to 5 wt% DMSO [8]. This ink enables stable printing over larger areas. By replacing DMSO with cyrene and GC, the conductivity can be improved by a factor of two. It is proposed that residual GC may be acting as a dopant, enhancing electrical properties of the PEDOT:PSS in a similar manner as DSMO, or as was demonstrated previously for glycerol-doped PEDOT:PSS [53], and supported by observation that variants of Ink_{CG} containing 4 wt% to 5 wt% GC had lower sheet resistances (Supplementary Information SI2, Fig. S1), were less stable in printing and presented features indicating gelation of the ink during drying. The influence of cyrene residues on PEDOT:PSS conductivity is yet unknown. Environmental and storage stability of the Ink_{CG} with respect to surface texture and electrical properties is comparable or better than that of DMSO based inks [54]. As such, Ink_{CG} can be successfully utilised in heterostructures, where stability against conditions required for processing and post deposition of subsequent layers is essential for device performance. The improved jetting stability of Ink_{CG} has demonstrated that this ink is suited to large-scale deposition of high-accuracy pattern arrays for heterostructure devices, competitive with the overall surface area of other recent large-scale demonstrations, while demonstrating improved pattern complexity [22], which was previously achieved with rapid prototyping of structural electronics [55]. Thus, Ink_{CG} presents solutions to future large-scale printing applications such as large transparent capacitive touch sensors, or large-scale parallel production of optoelectronics and sensors. The improved jetting stability opens up opportunities for Ink_{CG} to be multi-material IJ3DP co-printed with other functional and structural inks, to produce complex 3D-printed structures and heterostructures with high degree of design freedom, as needed for applications in electronic and optoelectronic devices.

4. Conclusion

In this work a novel formulation of PEDOT:PSS ink, Ink_{CG}, formulated using renewably sourced solvent cyrene and glycerol carbonate, as alternative to DMSO was demonstrated for use in additive manufacturing of electronic devices. Suppression of the coffee ring effect was achieved for this formulation and optimisation of the inkjet deposition strategy enabled deposition of PEDOT:PSS layers with waviness as low as $Sa = 16$ nm. Low roughness combined with stable electrical properties in different environments enabled production of PEDOT:PSS heterostructures with Ag nanoparticle ink and graphene ink, offering opportunities for future exploitation in heterostructure devices. In future work, carrier mobility and z-axis conductivity dependence of Ink_{CG} require study and characterisation of junction interactions with other inkjet printed electronic materials to develop fully IJ3DP printed functional devices, such as LEDs and solar cell. The reported here improved jetting stability achieved with the new formulation enables long term stable deposition of PEDOT:PSS can pave the way for inkjet manufacturing of complex 3D structures and devices, including bendable and flexible electronics.

CRediT authorship contribution statement

Geoffrey Rivers: Writing – review & editing, Writing – original draft, Methodology, Investigation, Conceptualization. **Jonathan S. Austin**: Writing – original draft, Methodology, Investigation. **Yinfeng He**: Writing – review & editing, Methodology, Conceptualization. **Adam Thompson**: Writing – review & editing, Methodology, Investigation. **Negar Gilani**: Investigation, Methodology, Writing – review & editing. **Nathan Roberts:** Writing – original draft, Methodology, Investigation. **Peng Zhao**: Writing – original draft, Software, Methodology, Formal analysis. **Christopher J. Tuck**: Writing – review & editing, Funding acquisition, Conceptualization. **Richard J.M. Hague**: Writing – review & editing, Funding acquisition, Conceptualization. **Ricky D Wildman.**: Writing – review & editing, Supervision, Resources, Funding acquisition, Conceptualization. **Lyudmila Turyanska**: Writing – review & editing, Methodology, Conceptualization.

Declaration of Competing Interest

The authors declare that they have no known competing financial interests or personal relationships that could have appeared to influence the work reported in this paper.

Data availability

Data will be made available on request.

Acknowledgements

This work is supported by the Engineering and Physical Sciences Research Council award "Enabling Next Generation Additive Manufacturing" [grant number EP/P031684/1]. AT and NR would also like to thank the UKRI Research England Development (RED) Fund via the Midlands Centre for Data-Driven Metrology. The authors thank Dr Michael W. Fay, Dr Christopher Parmenter, and the Nanoscale and Microscale Research Centre (nmRC) for electron microscopy studies, supported by the Engineering and Physical Sciences Research Council (EPSRC) [under grant EP/L022494/1] and the University of Nottingham. The authors thank NSERP undergraduate research assistant Noof Al Lawati for contributions to optical characterisation.

Appendix A. Supporting information

Supplementary data associated with this article can be found in the online version at doi:10.1016/j.addma.2023.103452.

References

[1] N.A.B. Zulkifli, M.A. Johar, O.M.F. Marwah, M.H.I. Ibrahim, Review on advances of functional material for additive manufacturing, IOP Conf. Ser. Mater. Sci. Eng. 226 (2017), 012177, https://doi.org/10.1088/1757-899X/226/1/012177.
[2] S. Vafaei, C. Tuck, R. Wildman, I. Ashcroft, Spreading of the nanofluid triple line in ink jet printed electronics tracks, Addit. Manuf. 11 (2016) 77–84, https://doi.org/10.1016/J.ADDMA.2016.04.005.

[3] J. Lin, Z. Zhu, C.F. Cheung, F. Yan, G. Li, Digital manufacturing of functional materials for wearable electronics, J. Mater. Chem. C 8 (2020) 10587–10603, https://doi.org/10.1039/D0TC01112F.

[4] L. Nayak, S. Mohanty, S.K. Nayak, A. Ramadoss, A review on inkjet printing of nanoparticle inks for flexible electronics, J. Mater. Chem. C 7 (2019) 8771–8795, https://doi.org/10.1039/C9TC01630A.

[5] N. Divakaran, J.P. Das, A.K.P. V, S. Mohanty, A. Ramadoss, S.K. Nayak, Comprehensive review on various additive manufacturing techniques and its implementation in electronic devices, J. Manuf. Syst. 62 (2022) 477–502, https://doi.org/10.1016/J.JMSY.2022.01.002.

[6] F. Zhang, E. Saleh, J. Vaithilingam, Y. Li, C.J. Tuck, R.J.M. Hague, R.D. Wildman, Y. He, Reactive material jetting of polyimide insulators for complex circuit board design, Addit. Manuf 25 (2019) 477–484, https://doi.org/10.1016/j.addma.2018.11.017.

[7] S. Kee, N. Kim, B. Park, B. Seong Kim, S. Hong, J.-H. Lee, S. Jeong, A. Kim, S.-Y. Jang, K. Lee, S. Kee, N. Kim, B. Park, B.S. Kim, S. Hong, J. Lee, S. Jeong, A. Kim, S. Jang, K. Lee, Highly deformable and see-through polymer light-emitting diodes with all-conducting-polymer electrodes, Adv. Mater. 30 (2018) 1703437, https://doi.org/10.1002/ADMA.201703437.

[8] E. Bihar, D. Corzo, T.C. Hidalgo, D. Rosas-Villalva, K.N. Salama, S. Inal, D. Baran, Fully inkjet-printed, ultrathin and conformable organic photovoltaics as power source based on cross-linked PEDOT:PSS electrodes, Adv. Mater. Technol. 5 (2020) 2000226, https://doi.org/10.1002/admt.202000226.

[9] Y. Zhu, T. Tang, S. Zhao, D. Joralmon, Z. Poit, B. Ahire, S. Keshav, A.R. Raje, J. Blair, Z. Zhang, X. Li, Recent advancements and applications in 3D printing of functional optics, Addit. Manuf. 52 (2022), 102682, https://doi.org/10.1016/J.ADDMA.2022.102682.

[10] G. Azzellino, A. Grimoldi, M. Binda, M. Caironi, D. Natali, M. Sampietro, Fully inkjet-printed organic photodetectors with high quantum yield, Adv. Mater. 25 (2013) 6829–6833, https://doi.org/10.1002/ADMA.201303473.

[11] E. Tan, A. Pappa, C. Pitsalidis, J. Nightingale, S. Wood, F.A. Castro, R.M. Owens, J. Kim, A highly sensitive molecular structural probe applied to in situ biosensing of metabolites using PEDOT:PSS, Biotechnol. Bioeng. 117 (2020) 291–299, https://doi.org/10.1002/bit.27187.

[12] A. Kalkal, S. Kumar, P. Kumar, R. Pradhan, M. Willander, G. Packirisamy, S. Kumar, B.D. Malhotra, Recent advances in 3D printing technologies for wearable (bio)sensors, Addit. Manuf. 46 (2021), 102088, https://doi.org/10.1016/J.ADDMA.2021.102088.

[13] S. Zhang, P. Kumar, A.S. Nouas, L. Fontaine, H. Tang, F. Cicoira, Solvent-induced changes in PEDOT:PSS films for organic electrochemical transistors, APL Mater. 3 (2015), 014911, https://doi.org/10.1063/1.4905154.

[14] L. Zhou, M. Yu, X. Chen, S. Nie, W.-Y. Lai, W. Su, Z. Cui, W. Huang, L. Zhou, M. Yu, W. Lai, W. Huang, X. Chen, S. Nie, W. Su, Z. Cui, Screen-printed poly(3,4-ethylenedioxythiophene):poly(styrenesulfonate) grids as ITO-free anodes for flexible organic light-emitting diodes, Adv. Funct. Mater. 28 (2018) 1705955, https://doi.org/10.1002/ADFM.201705955.

[15] S. Ashizawa, R. Horikawa, H. Okuzaki, Effects of solvent on carrier transport in poly(3,4-ethylenedioxythiophene)/poly(4-styrenesulfonate), Synth. Met. 153 (2005) 5–8, https://doi.org/10.1016/J.SYNTHMET.2005.07.214.

[16] L. Zhou, M. Yu, L. Yao, W.Y. Lai, Mayer rod-coated organic light-emitting devices: binary solvent inks, film topography optimization, and large-area fabrication, Adv. Eng. Mater. 24 (2022) 2101558, https://doi.org/10.1002/ADEM.202101558.

[17] N. Mkhize, H. Bhaskaran, Electrohydrodynamic jet printing: introductory concepts and considerations, Small Sci. 2 (2022) 2100073, https://doi.org/10.1002/SMSC.202100073.

[18] D. Li, W.Y. Lai, Y.Z. Zhang, W. Huang, Printable transparent conductive films for flexible electronics, Adv. Mater. (2018), https://doi.org/10.1002/adma.201704738.

[19] A. Singh, M. Katiyar, A. Garg, Understanding the formation of PEDOT:PSS films by ink-jet printing for organic solar cell applications, RSC Adv. 5 (2015) 78677–78685, https://doi.org/10.1039/C5RA11032G.

[20] P.D. Angelo, G.B. Cole, R.N. Sodhi, R.R. Farnood, Conductivity of inkjet-printed PEDOT:PSS-SWCNTs on uncoated papers, Nord. Pulp Pap. Res. J. 27 (2012) 486–495, https://doi.org/10.3183/npprj-2012-27-02-p486-495.

[21] P. Wilson, C. Lekakou, J. Watts, Electrical, morphological and electronic properties of inkjet printed PEDOT: PSS, in: 2012 12th IEEE Int. Conf. Nanotechnol., IEEE, 2012: pp. 1–6.

[22] E. Ramon, E. Sowade, C. Martínez-Domingo, K.Y. Mitra, A. Alcalde, R.R. Baumann, J. Carrabina, Large-scale fabrication of all-inkjet-printed resistors and WORM memories on flexible polymer films with high yield and stability, Flex. Print. Electron. 6 (2021), 015003, https://doi.org/10.1088/2058-8585/ABDB40.

[23] L. Zhou, X. Chen, W. Su, Z. Cui, W.-Y. Lai, L. Zhou, W.-Y. Lai, X. Chen, W.M. Su, Z. Cui, In-depth investigation of inkjet-printed silver electrodes over large-area: ink recipe, flow, and solidification, Adv. Mater. Interfaces. 9 (2022) 2102548, https://doi.org/10.1002/ADMI.202102548.

[24] A.H. Espera, J.R.C. Dizon, A.D. Valino, R.C. Advincula, Advancing flexible electronics and additive manufacturing, Jpn. J. Appl. Phys. 61 (2022) SE0803, https://doi.org/10.35848/1347-4065/AC621A.

[25] Y.G. Park, I. Yun, W.G. Chung, W. Park, D.H. Lee, J.U. Park, High-resolution 3d printing for electronics, Adv. Sci. 9 (2022) 2104623, https://doi.org/10.1002/ADVS.202104623.

[26] I. Lee, G.W. Kim, M. Yang, T.S. Kim, Simultaneously enhancing the cohesion and electrical conductivity of PEDOT:PSS conductive polymer films using DMSO additives, ACS Appl. Mater. Interfaces. 8 (2016) 302–310, https://doi.org/10.1021/ACSAMI.5B08753/SUPPL_FILE/AM5B08753_SI_001.PDF.

[27] B. Lu, H. Yuk, S. Lin, N. Jian, K. Qu, J. Xu, X. Zhao, Pure PEDOT:PSS hydrogels, Nat. Commun 10 (2019) 1–10, https://doi.org/10.1038/s41467-019-09003-5.

[28] Y. Kim, S. Yoo, J.H. Kim, Water-based highly stretchable PEDOT:PSS/nonionic WPU transparent electrode, Polymers 14 (2022) 949, https://doi.org/10.3390/POLYM14050949/S1.

[29] J. Dong, G. Portale, Role of the processing solvent on the electrical conductivity of PEDOT:PSS, Adv. Mater. Interfaces. 7 (2020) 2000641, https://doi.org/10.1002/ADMI.202000641.

[30] J.E. Camp, S.B. Nyamini, F.J. Scott, Cyrene™ is a green alternative to DMSO as a solvent for antibacterial drug discovery against ESKAPE pathogens, in: RSC Med. Chem., 11, 2020, pp. 111–117, https://doi.org/10.1039/C9MD00341J.

[31] M.O. Sonnati, S. Amigoni, E.P. Taffin De Givenchy, T. Darmanin, O. Choulet, F. Guittard, Glycerol carbonate as a versatile building block for tomorrow: synthesis, reactivity, properties and applications, Green Chem. 15 (2013) 283–306, https://doi.org/10.1039/c2gc36525a.

[32] Z. Zhou, L. Ruiz Cantu, X. Chen, M.R. Alexander, C.J. Roberts, R. Hague, C. Tuck, D. Irvine, R. Wildman, High-throughput characterization of fluid properties to predict droplet ejection for three-dimensional inkjet printing formulations, Addit. Manuf. (2019), 100792, https://doi.org/10.1016/j.addma.2019.100792.

[33] A. Rivadeneyra, J. Fernández-Salmerón, J. Banqueri, J.A. López-Villanueva, L. F. Capitan-Vallvey, A.J. Palma, A novel electrode structure compared with interdigitated electrodes as capacitive sensor, Sens. Actuators B Chem. 204 (2014) 552–560, https://doi.org/10.1016/J.SNB.2014.08.010.

[34] C. Gomez, C. Campanelli, R. Su, R. Leach, Surface-process correlation for an ink-jet printed transparent fluoroplastic, Surf. Topogr. Metrol. Prop. 8 (2020), 034002, https://doi.org/10.1088/2051-672X/ABAC1C.

[35] J. Petzing, J. Coupland, R. Leach, Good Practice Guide No. 116 The Measurement of Rough Surface, 2010. https://www.npl.co.uk/gpgs/coherence-scanning-interferometry.

[36] ISO - ISO 25178-2:2012 - Geometrical product specifications (GPS) — Surface texture: Areal — Part 2: Terms, definitions and surface texture parameters, (n.d.). https://www.iso.org/standard/42785.html (accessed March 14, 2022).

[37] F. Wang, J.H. Gosling, G.F. Trindade, G.A. Rance, O. Makarovsky, N.D. Cottam, Z. Kudrynskyi, A.G. Balanov, M.T. Greenaway, R.D. Wildman, R. Hague, C. Tuck, T.M. Fromhold, L. Turyanska, Inter-flake quantum transport of electrons and holes in inkjet-printed graphene devices, Adv. Funct. Mater. 31 (2021), https://doi.org/10.1002/adfm.202007478.

[38] H. He, L. Zhang, S. Yue, S. Yu, J. Wei, J. Ouyang, Enhancement in the mechanical stretchability of PEDOT:PSS films by compounds of multiple hydroxyl groups for their application as transparent stretchable conductors, Macromolecules. 54 (2021) 1234–1242, https://doi.org/10.1021/ACS.MACROMOL.0C02309/SUPPL_FILE/MA0C02309_SI_001.PDF.

[39] S.S. Yoon, D.Y. Khang, Roles of nonionic surfactant additives in PEDOT:PSS thin films, J. Phys. Chem. C 120 (2016) 29525–29532, https://doi.org/10.1021/ACS.JPCC.6B12043/SUPPL_FILE/JP6B12043_SI_001.PDF.

[40] A. Håkansson, S. Han, S. Wang, J. Lu, S. Braun, M. Fahlman, M. Berggren, X. Crispin, S. Fabiano, Effect of (3-glycidyloxypropyl)trimethoxysilane (GOPS) on the electrical properties of PEDOT:PSS films, J. Polym. Sci. Part B Polym. Phys. 55 (2017) 814–820, https://doi.org/10.1002/polb.24331.

[41] X. Crispin, F.L.E. Jakobsson, A. Crispin, P.C.M. Grim, § P. Andersson, A. Volodin, | C. Van, Haesendonck, | M. Van Der Auweraer, W.R. Salaneck, M. Berggren, The Origin of the High Conductivity of Poly(3,4-ethylenedioxythiophene)-Poly (styrenesulfonate) (PEDOT-PSS) Plastic Electrodes (2006), https://doi.org/10.1021/CM061032.

[42] P. Wilson, C. Lekakou, J.F. Watts, A comparative assessment of surface microstructure and electrical conductivity dependence on co-solvent addition in spin coated and inkjet printed poly(3,4-ethylenedioxythiophene):polystyrene sulphonate (PEDOT:PSS), Org. Electron. 13 (2012) 409–418, https://doi.org/10.1016/j.orgel.2011.11.011.

[43] C. Seo, D. Jang, J. Chae, S. Shin, Altering the coffee-ring effect by adding a surfactant-like viscous polymer solution, Sci. Reports 2017 (71) (2017) 7, 1–9. https://doi.org/10.1038/S41598-017-00497-X.

[44] W.K. Hsiao, G.D. Martin, I.M. Hutchings, Printing stable liquid tracks on a surface with finite receding contact angle, Langmuir. 30 (2014) 12447–12455, https://doi.org/10.1021/LA502490P/SUPPL_FILE/LA502490P_SI_004.AVI.

[45] ISO - ISO 4287:1997 - Geometrical Product Specifications (GPS) — Surface texture: Profile method — Terms, definitions and surface texture parameters, (n.d.). https://www.iso.org/standard/10132.html (accessed January 20, 2022).

[46] L. Ouyang, C. Musumeci, M.J. Jafari, T. Ederth, O. Inganäs, Imaging the phase separation between PEDOT and polyelectrolytes during processing of highly conductive PEDOT:PSS films, ACS Appl. Mater. Interfaces. 7 (2015) 19764–19773, https://doi.org/10.1021/acsami.5b05439.

[47] L. Mu, Z. Hu, Z. Zhong, C. Jiang, J. Wang, J. Peng, Y. Cao, Inkjet-printing line film with varied droplet-spacing, Org. Electron. 51 (2017) 308–313, https://doi.org/10.1016/j.orgel.2017.08.012.

[48] E. Saleh, F. Zhang, Y. He, J. Vaithilingam, J.L. Fernandez, R. Wildman, I. Ashcroft, R. Hague, P. Dickens, C. Tuck, 3D inkjet printing of electronics using UV conversion, Adv. Mater. Technol. 2 (2017) 1700134, https://doi.org/10.1002/ADMT.201700134.

[49] G.F. Trindade, F. Wang, J. Im, Y. He, A. Balogh, D. Scurr, I. Gilmore, M. Tiddia, E. Saleh, D. Pervan, L. Turyanska, C.J. Tuck, R. Wildman, R. Hague, C.J. Roberts, Residual polymer stabiliser causes anisotropic electrical conductivity during inkjet printing of metal nanoparticles, Commun. Mater. 21 (2) (2021) 1–10, https://doi.org/10.1038/S43246-021-00151-0.

[50] J. Im, G.F. Trindade, T.T. Quach, A. Sohaib, F. Wang, J. Austin, L. Turyanska, C. J. Roberts, R. Wildman, R. Hague, C. Tuck, Functionalized gold nanoparticles with

a cohesion enhancer for robust flexible electrodes, ACS Appl. Nano Mater. 5 (2022) 6708–6716, https://doi.org/10.1021/ACSANM.2C00742/ASSET/IMAGES/MEDIUM/AN2C00742_M001.GIF.

[51] P. Zhao, Y. He, G.F. Trindade, M. Baumers, D.J. Irvine, R.J.M. Hague, I.A. Ashcroft, R.D. Wildman, Modelling the influence of UV curing strategies for optimisation of inkjet based 3D printing, Mater. Des. 208 (2021), 109889, https://doi.org/10.1016/j.matdes.2021.109889.

[52] J.C. Yu, J.A. Hong, E.D. Jung, D. Bin Kim, S.M. Baek, S. Lee, S. Cho, S.S. Park, K. J. Choi, M.H. Song, Highly efficient and stable inverted perovskite solar cell employing PEDOT:GO composite layer as a hole transport layer, Sci. Rep. 81 (8) (2018) 1–9, https://doi.org/10.1038/S41598-018-19612-7.

[53] J.-F.(李建丰) Li, C.(赵创) Zhao, H.(张恒) Zhang, J.-F.(同军锋) Tong, P.(张鹏) Zhang, C.-Y.(杨春燕) Yang, Y.-J.(夏养君) Xia, D.-W.(范多旺) Fan, Improving the performance of perovskite solar cells with glycerol-doped PEDOT:PSS buffer layer*, in: Chin. Phys. B, 25, 2015, 028402, https://doi.org/10.1088/1674-1056/25/2/028402.

[54] S. Kee, H. Kim, S.H.K. Paleti, A. El Labban, M. Neophytou, A.H. Emwas, H. N. Alshareef, D. Baran, Highly stretchable and air-stable PEDOT:PSS/Ionic liquid composites for efficient organic thermoelectrics, Chem. Mater. 31 (2019) 3519–3526, https://doi.org/10.1021/ACS.CHEMMATER.9B00819/SUPPL_FILE/CM9B00819_SI_001.PDF.

[55] E. MacDonald, R. Salas, D. Espalin, M. Perez, E. Aguilera, D. Muse, R.B. Wicker, 3D printing for the rapid prototyping of structural electronics, IEEE Access 2 (2014) 234–242, https://doi.org/10.1109/ACCESS.2014.2311810.